Title

Dual effector population modification gene-drive strains of the African malaria mosquitoes, Anopheles gambiae and Anopheles coluzzii

Journal

Proceedings of the National Academy of Sciences of the United States of America, 120(29)

ISSN

0027-8424

Authors

Carballar-Lejarazú, Rebeca
Dong, Yuemei
Pham, Thai Binh
et al.

Publication Date

2023-07-18

DOI

10.1073/pnas.2221118120

PNAS RESEARCH ARTICLE | APPLIED BIOLOGICAL SCIENCES OPEN ACCESS

Dual effector population modification gene-drive strains of the African malaria mosquitoes, *Anopheles gambiae* and *Anopheles coluzzii*

Rebeca Carballar-Lejarazú[a,1], Yuemei Dong[b,1], Thai Binh Pham[a,1], Taylor Tushar[a,1], Rodrigo M. Corder[c,1], Agastya Mondal[c], Héctor M. Sánchez C.[c], Hsu-Feng Lee[a], John M. Marshall[c], George Dimopoulos[b], and Anthony A. James[a,d,2]

Contributed by Anthony A. James; received March 2, 2023; accepted June 5, 2023; reviewed by Luke Alphey and Jackson Champer

Proposed genetic approaches for reducing human malaria include population modification, which introduces genes into vector mosquitoes to reduce or prevent parasite transmission. We demonstrate the potential of Cas9/guide RNA (gRNA)–based gene-drive systems linked to dual antiparasite effector genes to spread rapidly through mosquito populations. Two strains have an autonomous gene-drive system coupled to dual anti-*Plasmodium falciparum* effector genes comprising single-chain variable fragment monoclonal antibodies targeting parasite ookinetes and sporozoites in the African malaria mosquitoes *Anopheles gambiae* (AgTP13) and *Anopheles coluzzii* (AcTP13). The gene-drive systems achieved full introduction within 3 to 6 mo after release in small cage trials. Life-table analyses revealed no fitness loads affecting AcTP13 gene-drive dynamics but AgTP13 males were less competitive than wild types. The effector molecules reduced significantly both parasite prevalence and infection intensities. These data supported transmission modeling of conceptual field releases in an island setting that shows meaningful epidemiological impacts at different sporozoite threshold levels (2.5 to 10 k) for human infection by reducing malaria incidence in optimal simulations by 50 to 90% within as few as 1 to 2 mo after a series of releases, and by ≥90% within 3 mo. Modeling outcomes for low sporozoite thresholds are sensitive to gene-drive system fitness loads, gametocytemia infection intensities during parasite challenges, and the formation of potentially drive-resistant genome target sites, extending the predicted times to achieve reduced incidence. TP13-based strains could be effective for malaria control strategies following validation of sporozoite transmission threshold numbers and testing field-derived parasite strains. These or similar strains are viable candidates for future field trials in a malaria-endemic region.

CRISPR-Cas9 | *Plasmodium falciparum* | single-chain antibodies | cage trials | parasite challenge assays

Significance

Novel genetic strategies for the malaria eradication agenda exploit Cas9/gRNA (guide RNA)-based autonomous gene-drive systems carrying antiparasite effector genes, and these effectively reduce prevalence and numbers of the human parasite, *Plasmodium falciparum*, in the African malaria mosquitoes, *Anopheles gambiae* and *Anopheles coluzzii*. Results from laboratory assessments of population gene-drive dynamics, transgene genetic loads, and parasite suppression efficacy informed modeling of conceptual field releases that show that hypothetical strains based on the empirical data could have a meaningful epidemiological impact in reducing human incidence by 50 to 90%.

Malaria control efforts contributed significantly to reductions in human morbidity and mortality in the first 15 y of the 21st century (1). Preventative and therapeutic drugs and antivector measures had beneficial impacts that resulted in malaria elimination in several countries. However, these gains were dampened over the last several years and malaria cases in some regions are on the rise (2, 3). Additional tools are required to reduce malaria that persists in many areas due to environmental and socioeconomical conditions, and vaccines and novel genetics-based vector technologies are expected to contribute significantly (4, 5).

Genetics-based vector population modification approaches (also called "replacement") involve introducing genes that prevent parasite transmission into wild mosquito populations and have several predicted attractive features (6, 7). In addition to sustainability, they leave no "empty" ecological niche open to invasive species, and thus may be neutral in their environmental impact. Malaria control is likely to continue to be constrained by resources, and population modification tools could contribute to a serial approach in which malaria is eliminated in one locale and efforts then can be moved to a new region with the confidence that the previously treated area would remain free of parasites, thus consolidating elimination gains on the path to eradication.

The toolset to genetically engineer mosquitoes for population modification includes transformation techniques (8, 9), gene-drive systems (10–12), potent antiparasite effector molecules (13–18), standardized laboratory methods for evaluating strain efficacy (11, 17, 19–22), and modeling platforms (23, 24). We describe here the design, production, and testing of a gene-drive system, TP13, carrying an autonomous Cas9/gRNA (guide RNA)-based drive component [AgNosCd-1; (11)] linked to two genes that encode single-chain variable fragment monoclonal antibodies (scFvs) that target *Plasmodium falciparum* ookinetes and sporozoites, in genetically engineered strains of the African malaria

Author contributions: R.C.-L., Y.D., J.M.M., G.D., and A.A.J. designed research; R.C.-L., Y.D., T.B.P., T.T., R.M.C., and H.-F.L. performed research; R.C.-L., Y.D., T.B.P., T.T., R.M.C., A.M., H.M.S.C., J.M.M., G.D., and A.A.J. analyzed data; and R.C.-L., Y.D., T.B.P., T.T., J.M.M., G.D., and A.A.J. wrote the paper.

Reviewers: L.A., Pirbright Institute; and J.C., Peking University.

Competing interest statement: J.M.M. co-authored reviews with both reviewers.

[1]R.C.-L., Y.D., T.B.P., T.T., and R.M.C. contributed equally to this work.

[2]To whom correspondence may be addressed. Email: aajames@uci.edu.

This article contains supporting information online at https://www.pnas.org/lookup/suppl/doi:10.1073/pnas.2221118120/-/DCSupplemental.

Published July 10, 2023.

mosquitoes *Anopheles gambiae* (AgTP13) and *Anopheles coluzzii* (AcTP13).

Development guidelines for these strains call for phased testing during which specific criteria, including those addressing special challenges of gene-drive systems, must be met before moving from one phase to the next (25–27). These criteria are components of a target product profile (TPP) with listed ideal characteristics and minimally acceptable thresholds defined to assist "go/no-go" decision-making (7). We test and model here both entomological (gene-drive efficiency and fitness) and epidemiological (effector molecule efficacy and impact on transmission) criteria as part of the phased assessment of TP13-based gene-drive strains.

Gene-drive efficiency analyses focus on the rate of conversion ["homing rate" (23, 24)] of hemizygous to homozygous germline progenitor cells and the production of potential drive-resistant alleles (10–12, 28). In addition, the population-wide spread of a gene-drive system is likely to be affected by fitness loads resulting from integration of the system into the target chromosome (insertion/position effects) and the activity of the transgene components (expression effects) that may affect gene-drive mosquito reproductive competitiveness (29).

A robust epidemiological impact requires efficient antiparasite effector molecules that reduce human malaria incidence (rate of new infections) and prevalence (percentage of infected individuals). This can be achieved by reductions in parasite prevalence and intensities of infection (mean and/or median number of parasites in infected mosquitoes) in the vectors. A data-informed model predicted that transmission-blocking interventions that reduce oocyst prevalence ≥32% in three successive transmission cycles in a rodent model system (*P. berghei*) could lead to malaria elimination if the number (1-2) of infectious mosquito bites is low (30). While animal models may not translate directly to human transmission, they do provide initial benchmarks for comparative work. The proportion of *infected* mosquitoes may not be equivalent to the proportion of *infectious* mosquitoes. While early studies showed that direct inoculation of low numbers of human parasites (*Plasmodium vivax*) or low intensities of infection in an avian model (*Plasmodium gallinaceum*) can cause malaria (31, 32), recent experiments in model rodents and meta-analyses of data from human and animal parasite infection studies show a nonlinear relationship between mosquito parasite levels and a resulting vertebrate host infection following a bite from an infected mosquito (33, 34). Levels of <10,000 sporozoites in mosquito salivary glands significantly decreased the probability of subsequent infection. Furthermore, an expert panel recommended a reduction of 20 to 50% in human incidence as the minimally acceptable target for a population modification strain to be eligible for field testing (35). These thresholds are not likely to be related linearly to epidemiological impacts, and with the difficulty of testing them in human challenge trials, modeling should provide a practical alternative (36). The laboratory analyses and modeling done here support the further development of TP13-based strains for population modification as part of a comprehensive malaria control strategy.

Results

Design and Construction of AgTP13. The AgTP13 strain was generated by Cas9/gRNA-mediated chromosomal integration into the *Anopheles gambiae cardinal* gene locus (*Agcd*) of the gene-drive elements and effector molecules contained in the pTP13 plasmid (Fig. 1*A* and *SI Appendix*, *Materials and Methods*). pTP13 is derived from the pCO37 plasmid used in the *A. gambiae* gene-drive line, AgNosCd-1 (11). pTP13 has the pCO37 gene-drive components linked to two antiparasite effector scFvs, m1C3 and m2A10, targeting *P. falciparum* ookinetes and sporozoites, respectively, and regulated, respectively, by the *A. gambiae Carboxypeptidase A* [*AgCPA*, (Cp)] and *A. stephensi Vitellogenin 1* [*AsVg1*, (Vg)] promoters and 5- and 3-end untranslated regions (10, 16). The expression of both native genes is induced in adult females at different times following a blood meal although variations in stage-, tissue-, and sex-specificity are seen in transgenic mosquitoes utilizing their promoters (10, 16). The cyan fluorescent protein (CFP) gene serves as a dominant marker for the presence of the gene-drive system. pTP13 is ~20 kilobase pairs (kb) in length, of which ~15.6 kb comprises the drive system components, dominant marker gene, and scFvs.

pTP13 was coinjected with SpCas9 protein into 2,740 wild-type *A. gambiae* X1 embryos (WT-X1) derived from the G3 laboratory strain (37). G3 [MRA-112 (38)] was colonized from the Gambia in 1975 and is an *A. gambiae ss*/*A. coluzzii* hybrid (39). The gRNAs are provided by sequences encoded in the injected plasmid. The 1,094 (~40%) surviving G_0 adults were outcrossed to WT-X1 individuals of the opposite sex and 21 (0.36%, 21/5,906) G_1 larvae were CFP positive (CFP^+). Sixteen CFP^+ G_1 larvae survived to adulthood, and 10, six males and four females, produced viable progeny and were used to establish AgTP13.

AgTP13 Initial Characterization.

Genome integration. Sequencing genomic DNA amplicons of the junction sites derived from transgenic progeny from outcrossed (OX) and intercrossed (IX) individuals confirmed TP13 integration

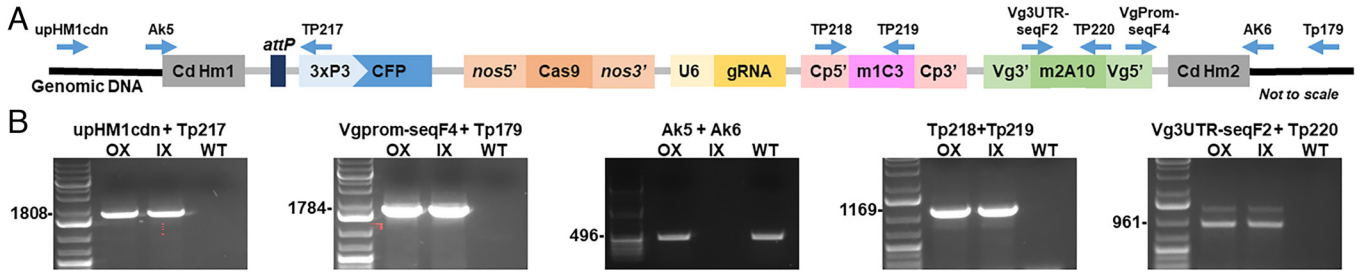

Fig. 1. Schematic representation and molecular validation of AgTP13. (*A*) Gene-drive system components. The components include the left- and right-homology arms (gray boxes, *cd* Hm1, *cd* Hm2) complementary to the endogenous *cd* gene (black line, Genomic DNA), a *ϕC31 attachment P* site (dark blue box, *attP*), the dominant cyan fluorescent protein eye marker cassette (lighter-blue boxes, 3×P3, CFP), the *nanos*-Cas9 nuclease cassette (orange-shaded boxes, *nos*5′ and *nos*3′, Cas9), the U6 guide RNA cassette (light-yellow boxes, U6, gRNA), the carboxypeptidase-encoding gene control DNA driving the m1C3 scFv (pink boxes, Cp5′ and Cp3′, m1C3), and the vitellogenin-encoding gene control DNA driving the m2A10 scFv (green boxes, Vg5′ and Vg3′, m2A10). Oligonucleotide primer names (*SI Appendix*, Table S1), orientations, and approximate locations are indicated with blue arrows (above). (*B*) Gene amplification analyses of the integrated AgTP13 gene-drive system. Gel electrophoresis and staining images (left to right) of amplicons between the left junction and cargo, right junction and cargo, left and right junction, and 5′- and 3′-end UTRs of the two antiparasite effector genes. Oligonucleotide primer pairs are listed above each image, and the source of the genomic DNA template is indicated [outcross (OX), intercross (IX), and wild-type (WT) control DNA]. Expected amplicon sizes in base pairs verified by DNA sequencing are listed on the left side of each gel image.

at the targeted *Agcd* gRNA cleavage site (Fig. 1*B* and *SI Appendix*, Fig. S1 and Table S1).

Effector gene expression. Gene amplification–based analyses (RT-PCR) of m1C3 and m2A10 expression at 0, 4, 12, 24, and 48 hours post blood meal (hPBM) used total RNA isolated from midguts and carcasses (all tissues except midguts) from hemizygous (carrying one copy of the gene-drive system) transgenic AgTP13 females as templates (*SI Appendix*, Fig. S2). The m1C3 transcripts are present in nonfed female midguts, but their abundance increased after a blood meal with the strongest signal at 4 hPBM, potentially increasing the amount of the gene product available to interact with its parasite target. Similarly, m2A10 transcripts were detectable in carcasses prior to blood feeding, but had their strongest signal at 24 hPBM.

Gene-drive validation. The six G_1 males and four G_1 females used to establish AgTP13 were first pool-mated in the presence of 178 WT-X1 females. The G_1 males were removed subsequently and outcrossed to 164 WT-X1 females. Both crosses showed high drive inheritance with 99.3% (441/444) and 100% (127/127) of the G_2 progeny from the pool and outcross, respectively, carrying a copy of the drive (CFP^+, *SI Appendix*, Table S2). The male and female CFP^+ G_2 progeny from the pool were intercrossed, while CFP^+ G_2 males from the outcross were removed as virgins and outcrossed again to WT-X1 females. Two subsequent generations of IX and OX progeny displayed high drive (range: 98 to 100%) and these were used to establish homozygous and hemizygous AgTP13 lines. Homozygous lines have both copies of *Agcd* ablated, resulting in larvae, pupae, and recently emerged adults (≤24 h post eclosion) having a red-eye (cd^-) phenotype (11).

AcTP13 Initial Characterization. The TP13 gene-drive system was introgressed into the long-colonized *A. coluzzii* Mopti strain [WT-Mopti; MRA-763 (38)] to evaluate its performance in a sibling species in the *A. gambiae sensu lato* complex. Fifty homozygous CFP^+/cd^- male AgTP13 were outcrossed to 50 WT-Mopti females. Black eye (CFP^+/cd^+) hybrid male progeny were recovered and backcrossed to WT-Mopti females. This mating scheme was repeated for five generations, yielding a line in which females theoretically carry ~97% of the WT-Mopti genome with the exception of the Y chromosome, which was conserved from *A. gambaie*. AcTP13 was maintained as both homozygous and hemizygous lines and showed qualitatively greater constitutive and ectopic m1C3 and m2A10 expression than AgTP13, verifying that the genes are present and functional (*SI Appendix*, Fig. S2). AgNosCd-1 was introgressed similarly into WT-Mopti to generate AcNosCd-1.

AgTP13 and AcTP13 Gene-Drive Properties.

Male and female lineage gene-drive dynamics. Male- and female-derived AgTP13 and AcTP13 lineages were assessed for possible sex-specific differences in drive efficiency detectable in the inheritance of the gene-drive system and emergence of mutations resulting from Cas9/gRNA-induced, nonhomologous end-joining (NHEJ) (10, 11, 28). Fifty each of hemizygous AgTP13 and AcTP13 males and females were outcrossed in three biological replicates to WT-X1 and WT-Mopti mosquitoes, respectively, of the opposite sex. As seen with AgNosCd-1 (11), male AgTP13 lineages have higher drive inheritance, 99.5 to 100%, than female lineages, 85.5 to 96.9% ($\chi^2 = 174.9$, $P < 0.0001$), and the drive inheritance over two generations in both lineages is similar to that of the drive-only AgNosCd-1 (Table 1). AcTP13 showed no differences between male and female lineages ($\chi^2 = 0.15$, d.f. = 1, $P = 0.70$), with drive inheritance ranging from 97.5 to 100% for both sexes over two generations, well within the range observed with AgTP13 and AcNosCd-1 (*SI Appendix*, Tables S2 and S3). The exceptional *cardinal* eye phenotype (CFP^+/cd^-), which should not be generated from an outcross unless an NHEJ mutation of *Agcd* occured during reproduction, was observed in a small proportion (0.15 to 0.9%) of all progeny from hemizygous AgTP13 and AcTP13 female parents (Table 1). AgTP13 female lineages did not generate a greater proportion of CFP^+/cd^- progeny when compared with AgNosCd-1 female lineages; however, this phenotype was observed more often among the individual mating events with 3/3 of the AgTP13 female parent outcrosses generating exceptional phenotype progeny compared to 4/8 of the AgNosCd-1 female parent outcrosses. AcTP13 also generated CFP^+/cd^- progeny in the female lineages; however, the proportion of these (range from 0.4 to 0.9%, with the highest found in successive female lineages) was similar to AgNosCd-1, AgTP13, and AcNosCd-1 [Table 1 and *SI Appendix*, Table S3; (11)].

Table 1. Gene-drive and eye phenotypes from male- and female-derived AgTP13 and AcTP13 lineages*

Gen	AgTP13				AcTP13			
P	Male-founder lineages†		Female-founder lineages†		Male-founder lineages†		Female-founder lineages†	
	CFP^+ progeny‡							
F_1	♂ 100% (1,413/1,413)		♀ 96.9% (1,172/1,209)		♂ 97.4% (1,016/1,043)		♀ 97.8% (1,472/1,507)	
F_2	♂ 99.5% (189/190)	♀ 94.9% (1,198/1,263)	♂ 99.5% (1,049/1,054)	♀ 85.5% (799/935)	♂ 100% (165/165)	♀ 100% (176/176)	♂ 100% (235/235)	♀ 97.5% (197/202)
	cardinal-eye progeny§							
F_1	♂ 0% (0/1,413)		♀ 0.5% (6/1,209)		♂ 0% (0/1,043)		♀ 0.4% (6/1,507)	
F_2	♂ 0% (0/190)	♀ 0.15% (2/1,263)	♂ 0% (0/1,054)	♀ 0.2% (2/935)	♂ 0% (0/165)	♀ 0.5% (1/176)	♂ 0% (0/235)	♀ 0.9% (5/202)
	Tear-eye (mosaic) progeny¶							
F_1	♂ 0.4% (6/1,413)		♀ 13.9% (168/1,209)		♂ 1.5% (16/1,043)		♀ 4.7% (71/1,507)	
F_2	♂ 0% (0/190)	♀ 5.2% (66/1,263)	♂ 0.6% (6/1,054)	♀ 4.2% (39/935)	♂ 0.6% (1/165)	♀ 4.5% (8/176)	♂ 0.4% (1/235)	♀ 5.9% (12/202)

*Hemizygous AgTP13, AcNosCd-1, and AcTP13 males and females outcrossed with WT mosquitoes of the opposite sex of the same species in a 1:1 ratio of 50 males to 50 females. The data are pooled from three independent replicates.
†Symbols refer to the sex (♂ male, ♀ female) of the gene-drive parents in the parental (P) and progeny (F_1, F_2) generations.
‡Percentage of total progeny expressing the CFP marker gene.
§Percentage of the total progeny with heteroallelic phenotypes comprising one copy of the drive element (CFP^+) and one resistant mutant *cardinal* (cd^-) allele.
¶Percentage of the total progeny with the tear (mosaic-eye) phenotypes.

Maternal effects. Drive-carrying females deposit Cas9/gRNA complexes into their developing oocytes that can act on incoming male chromosomes and affect both germline and somatic cells of the resulting embryos (10, 11, 28, 40). Along with possible somatic expression of the drive system, this can result in mutations that produce a phenotype, "tear," visible in the eyes of pupal and adult insects (11). Tear eyes have patches of ommatidia with multiple colors that may include the wild type (black eye) and one or more versions of a *cardinal* phenotype (red- to near-white eye). Molecular analyses support the conclusion that this phenotype results from genotypically distinct, homozygous or heteroallelic combinations of nonfunctional mutations in clonally related groups of adjacent cells to form a mosaic eye (10, 11). These mosaics and other exceptional phenotypes (unexpected combinations of CFP^+ or CFP^- individuals with wild type or red eyes) permit monitoring both germline and somatic NHEJ events.

Homozygous drive females are expected to deposit more Cas9/gRNA complexes than those of hemizygotes, which can lead to a higher likelihood of NHEJ events in wild-type alleles and result in an increased incidence of mutations in their offspring. Homo- and hemizygous AgTP13 and AcTP13 females were outcrossed to WT-X1 and WT-Mopti males, respectively, and the numbers of exceptional CFP^+/cd^- progeny were recorded (*SI Appendix*, Table S4). Homozygous AgTP13 females generated a greater proportion of CFP^+/cd^- offspring (average of 4.6%) compared to hemizygous AgTP13 (0.15 to 0.5%; Table 1), a result consistent with AgNosCd-1 females (28). Similar proportions were observed in AcTP13 with 5.1% and 0.4 to 0.9% CFP^+/cd^- from homo- and hemizygotes, respectively (Table 1 and *SI Appendix*, Table S4) and AcNosCd-1 with 6.0% and 1.1-1.3% from homo- and hemizygotes, respectively (*SI Appendix*, Tables S3 and S5).

Intercrosses of the CFP^+/cd^- and CFP^+/tear-eye F1 progeny were performed to evaluate whether the mutant alleles would inhibit drive dynamics (*SI Appendix*, Table S4). The CFP^+/cd^- intercross had a reduction in drive inheritance in both AgTP13 and AcTP13 (80.6% and 82.2% CFP^+ progeny, respectively), but did not result in a return to Mendelian inheritance ratios (AgTP13, $\chi^2 = 7.9$, d.f. = 1, $P < 0.01$; AcTP13, $\chi^2 = 5.6$, d.f. = 1, $P < 0.05$). The CFP^+/tear-eye intercrosses revealed strong drive activity in both AgTP13 and AcTP13 (99.6% for both) similar to the tear individuals from the AgNosCd-1 line, and these combined data support the conclusion that this phenotype results from somatic as opposed to germline mutations (11, 28).

Population gene-drive dynamics. Discrete, nonoverlapping cage trials with 1:1 and 1:3 release ratios of gene-drive, AgTP13 and AcTP13, to wild-type males were set up in triplicate. For the 1:1 ratio, 75 homozygous gene-drive males were seeded with 75 WT males (WT-X1 for AgTP13, and WT-Mopti for AcTP13) and 150 each of the corresponding virgin females (cages AgTP13-A1, A2, A3 and AcTP13-A1, A2, A3). The 1:3 ratio had 37 homozygous transgenic males seeded with 111 WT males and 150 each of the corresponding virgin females (cages AgTP13-B1, B2, B3 and AcTP13-B1, B2, B3). Three hundred randomly selected G_1 second-instar (L2) larvae from each cage were removed to a new cage for the subsequent generations, and an additional 600 randomly selected L2 larvae were reared separately for sexing and phenotypic screening. A total of 404,072 mosquitoes were scored in the combined cage trial experiments (*SI Appendix*, Tables S6–S17).

The percentage of first-generation (G_1) CFP^+ mosquitoes in the 1:1 ratio trial is expected to be 50% (1/2 chance of parental females mating with homozygous transgenic males). G_1 larvae from all three AgTP13 replicates had CFP^+ percentages, 25.7% (155/603, A1), 22.7% (131/578, A2), and 10.6% (65/616, A3), significantly lower than expected [$X^2 = 349.7$, d.f. = 2, ($P < 0.0001$)] (Fig. 2 and *SI Appendix*, Fig. S3 and Tables S6–S8). In contrast, significantly higher CFP^+ offspring were observed for AcTP13 1:1 ratio replicates [$X^2 = 47.0$, d.f. = 2, ($P < 0.0001$)] with 58.4% (286/490, A1), 64.1% (390/608, A2), and 63.9% (262/410, A3) (Fig. 2 and *SI Appendix*, Fig. S3 and Tables S9–S11).

The percentages of CFP^+ mosquitoes increased in all subsequent generations for both AgTP13 and AcTP13 with a faster rate observed in the latter. All the three 1:1 AcTP13 replicates reached full introduction (100% CFP^+; every mosquito having at least one copy of TP13) at the third generation (G_3) (Fig. 2 and *SI Appendix*, Fig. S3 and Tables S9–S11). AgTP13 cages achieved full introduction as early as G_6 for cage A1 and G_7 for A2 (Fig. 2 and *SI Appendix*, Fig. S3 and Tables S6–S8). AgTP13-A3 reached a peak of ~95% CFP^+ at G_7 and then declined as mutant, drive-resistant alleles accumulated in the population. The AgTP13 rate of full introduction was slower than that of AgNosCd-1 (Fig. 2 and *SI Appendix*, Fig. S3, (11)]. Homozygosity (CFP^+/cd^-) for the drive system in some mosquitoes was seen first in G_2 for all AgTP13 and AcTP13 1:1 release-ratio cages, and all three AcTP13 replicates were 100% CFP^+/cd^- at G_4 (Fig. 2 and *SI Appendix*, Fig. S3 and Tables S9–S11). It is possible that a small fraction of the CFP^+/cd^- mosquitoes may be hemizygous for the gene drive–containing allele and a nonfunctional NHEJ *cardinal* allele (Table 1).

The percentage of G_1 CFP^+ progeny in the 1:3 cages is expected to be 25% (1/4 chance of parental females mating with homozygous transgenic males). Similar to the 1:1 release ratio, AgTP13 larvae from all the three replicates had significantly lower CFP^+ G_1 percentages, 4.37% (15/343, B1), 5.04% (17/337, B2), and 5.43% (21/387, B3) [$X^2 = 171.6$, d.f. = 2, ($P < 0.0001$)] (Fig. 2 and *SI Appendix*, Fig. S3 and Tables S12–S14). In contrast, the 1:3 AcTP13 replicates showed significantly higher CFP^+ G_1 percentages: 26.0% (156/600, B1), 36.1% (228/631, B2), and 38.2% (262/686, B3) [$X^2 = 79.7$, d.f. = 2, ($P < 0.0001$)] (Fig. 2 and *SI Appendix*, Fig. S3 and Tables S15–S17).

AcTP13 continued to demonstrate excellent cage trial results as all the three 1:3 release-ratio replicates reached full introduction (100% CFP^+) at G_4, and 100% homozygosity (CFP^+/cd^-) at G_5 (Fig. 2 and *SI Appendix*, Fig. S3 and Tables S15–S17). In contrast, only AgTP13-B2 reached full introduction at G_6. Cages B1 and B3 reached maximum values of ~97% (G_{10}) and ~95% (G_8), respectively (Fig. 2 and *SI Appendix*, Fig. S3 and Tables S12–S14). Furthermore, maximum introduction waned in all the three cages in later generations (G_9 to G_{11}), reaching a low of ~61% in B3.

Population sizes fluctuated among the cages and generations with the AgTP13 1:1 release-ratio cages averaging 2,694 (A1), 2,761 (A2), and 3,336 (A3) (*SI Appendix*, Fig. S3 and Tables S6–S8), and AcTP13 1:1 4,447 (A1), 4,502 (A2), and 4,631 (A3) mosquitoes per generation (excluding cage founders) (*SI Appendix*, Fig. S2 and Tables S9–S11). The AgTP13 1:3 cages fluctuated similarly with averages of 3,545 (B1), 2,676 (B2), and 3,638 (B3) mosquitoes per generation, whereas AcTP13 cages had higher averages of 6,633 (B1), 5,743 (B2), and 5,674 (B3) (Fig. 2 and *SI Appendix*, Fig. S3 and Tables S12–S15).

Cage trial data were used to parameterize a model of gene-drive dynamics that accounts for drive inheritance, resistance-allele formation, and fitness parameters for different genotypes (23). The genotypes include four possible *Agcd* alleles, an intact gene-drive (homing) allele ("H;" the TP13 gene cassette conferring the CFP^+ phenotype), a wild-type allele ("W," cd^+; conferring a wild-type, black-eye, phenotype), a functional, potential drive-resistant *Agcd* allele ("R," cd^+; an in-frame gRNA target-site mutation conferring a wild-type, black-eye, phenotype), and a nonfunctional, potential drive-resistant allele ("B" cd^-, a gRNA target-site mutation conferring a *cardinal*, red-eye phenotype in a homozygote, heteroallelic

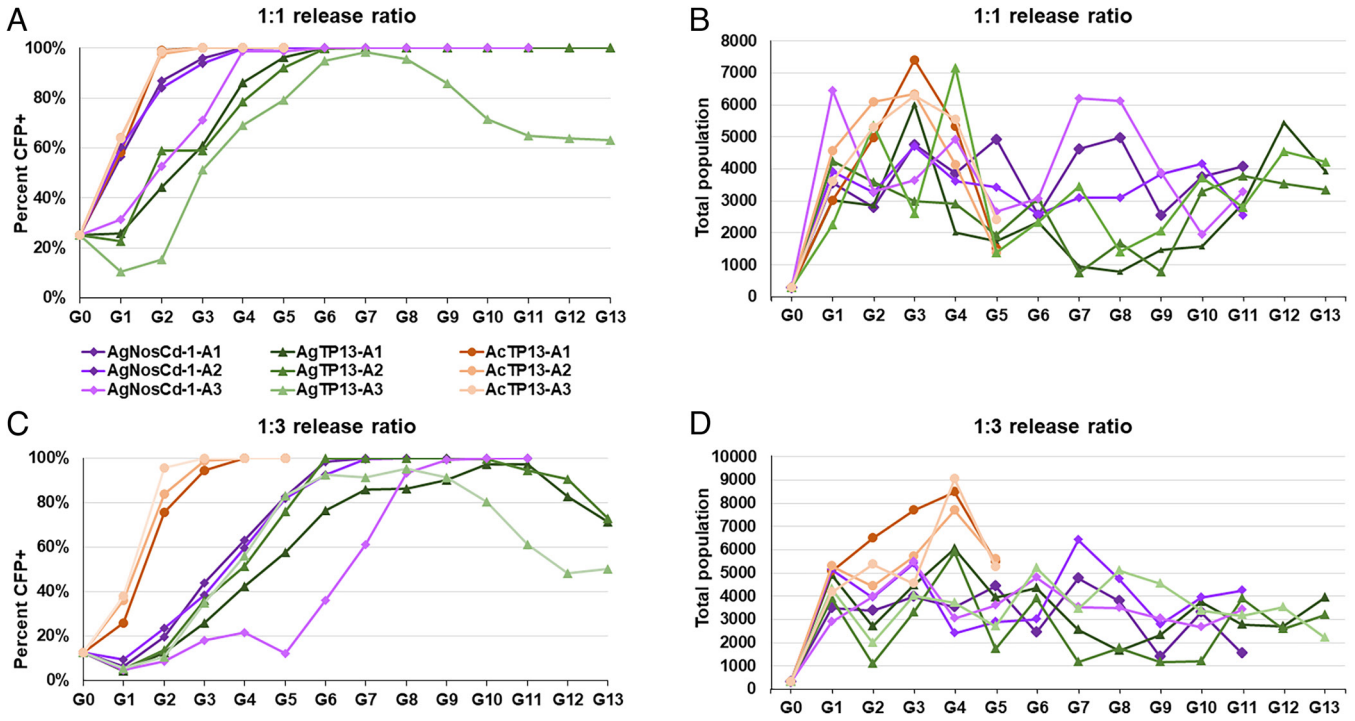

Fig. 2. Gene-drive dynamic of AgTP13, AcTP13, and AgNosCd-1 in discrete, nonoverlapping generation small cage trial with 1:1 and 1:3 release ratios of gene-drive to wild-type males. (*A*) Two sets of triplicate cages (0.005 m^3), denoted AgTP13-A1, A2, A3 and AcTP13-A1, A2, A3, were seeded with 75 homozygous transgenic (AgTP13 or AcTP13) and 75 WT males (WT-X1 or WT-Mopti) (1:1 ratio) along with 150 WT females of the respective parental strain. The resulting next-generation progeny were scored for the dominant cyan fluorescent protein, CFP^+, and *cardinal* eye-color phenotype. AgTP13 drive dynamics (green-shaded lines, triangle marker) and AcTP13 drive dynamics (orange-shaded lines, circle marker) compared with AgNosCd-1 (purple-shaded lines, diamond marker; data from cages A1, A2, and A3 in ref. 11. Percentages of CFP^+ mosquitoes (*y* axis) in the total population of each cage were scored at each generation (*x* axis). (*B*) Total population sizes of AgTP13 and AcTP13 cages at each generation compared to AgNosCd-1 [cages A1, A2, and A3 in ref. 11. (*C*) Two sets of triplicate cages, denoted AgTP13-B1, B2, B3 or AcTP13-B1, B2, B3, were seeded with 37 homozygous transgenics (AgTP13 or AcTP13) and 111 WT males (WT-X1 or WT-Mopti) (1:3) ratio] along with 150 WT females of the respective parental strain. Next-generation progeny scored and presented as in *A*. (*D*) Total population sizes presented as in *B*. AgNosCd-1 population size data from cages B1, B2, and B3 in ref. 11.

combination of nonfunctional alleles or opposite an H allele) (*SI Appendix*, Table S18). A stochastic implementation of the fitted model that qualitatively compared the time-series of model-predicted genotype frequencies was consistent with the empirical outcomes of the cage experiments and high-efficiency gene-drive (*SI Appendix*, Figs. S4 and S5).

Mosquitoes with exceptional phenotypes were recovered only from the AgTP13 1:1 and 1:3 release-ratio cages and include CFP^-/cd^- (no marker gene, *cd* red-eye phenotype) from all generations, and CFP^-/cd^+ [no marker gene, black-eye (WT) phenotype] and CFP^+/cd^+ [marker gene, black-eye (WT) phenotype] at later generations. Molecular analyses of the CFP^+/cd^+ individuals revealed genotypes comprising a drive allele with either a WT or in-frame functional NHEJ allele (*SI Appendix*, Tables S19 and S20). The AgTP13-A3 CFP^-/cd^+ individuals had two in-frame mutant *cd* alleles and the CFP^-/cd^- individual had one out-of-frame allele, both genotypes first detected in G_7 and persisting for subsequent generations. Most AgTP13-B3 CFP^+/cd^+ and CFP^-/cd^+ have at least one WT allele at G_8 and G_9 and the frequency of these declined by G_{10} and G_{11} with a concomitant increase of in-frame and out-of-frame insertion and deletion (indel) alleles (*SI Appendix*, Table S9). In addition, most CFP^+/cd^+ and CFP^-/cd^+ mosquitoes have at least one in-frame allele, and all have the same in-frame allele through G_8 to G_{11}, consistent with the inheritance of this identified NHEJ allele (*SI Appendix*, Tables S19 and S20).

Life-table parameters. Aggregate male fitness was evaluated as the "likelihood to contribute to the next generation" and is determined by the frequencies of the CFP^+ phenotype in the first-generation progeny of an outcross in which gene-drive and WT males compete for mating with WT females (11, 19). A 1:1 ratio of gene drive to WT males revealed a significant difference between homozygous AgTP13 and WT males contributing to the next generation (χ^2 = 1,045.3, d.f. = 1, N = 3,190, $P < 0.00001$; *SI Appendix*, Table S21 and S22). The average percentage of CFP^+ progeny in three replicate crosses in a one-generation trial, 22.4%, is far below the 50% expected if AgTP13 males were as competitive as WT, consistent with the observed frequency of G_1 CFP^+ progeny in the 1:1 cage-trial replicates. No significant difference was observed for hemizygous males (χ^2 = 0.041, d.f. = 1, N = 3,269, P = 0.84), where the average percentage of CFP^+ progeny in three replicates was 48.8%. This reflects the high efficiency of gene drive in the male germline, which results in nearly all of the sperm (99.5 to 100%) carrying the gene-drive insertion while the somatic tissues remain hemizygous. In contrast, homozygous AcTP13 males were as likely to contribute as their wild-type competitors (51.2%, χ^2 = 2.4, d.f. = 1, N = 3,573, P = 0.12) and hemizygotes were more likely to contribute (64.1%, χ^2 = 268, d.f. = 1, N = 3,397, $P < 0.0001$).

Homozygous AgTP13 males had a significantly lower median lifespan (11 d) than both hemizygous AgTP13 (38 d) and WT-X1 males (36 d) ($P < 0.00001$; *SI Appendix*, Table S21 and S22). However, both homozygous (37 d; $P < 0.0001$) and hemizygous (33 d; P = 0.029) AcTP13 males had a higher median lifespan than that of WT-Mopti (29 d). No significant differences were observed in the lifespan of AgTP13 and WT-X1 females; similar to homozygous AcTP13 males, homozygous AcTP13 females had a higher median lifespan (33 d; $P \leq 0.012$) than hemizygous AcTP13 (25 d) or WT-Mopti (29 d) females. All larval and pupal counts include the sum of both males and females in each sample. Homozygous AgTP13 have shorter larval and pupal development times compared with AgTP13 hemizygotes and WT ($P < 0.0001$). Both AcTP13

homozygotes and hemizygotes have slightly shorter larval and pupal development times when compared to WT-Mopti ($P \leq 0.006$). AgTP13 homozygotes had reduced larval survival (72%) as did AgTP13 hemizygotes (78%) when compared to WT X1 (83%) ($P \leq 0.0055$). Larval viability for both AcTP13 homozygotes (73%) and hemizygotes (78%) was greater than that of the control WT-Mopti (62%) ($P \leq 0.0001$). AgTP13 homozygous females produced more eggs (117) than the AgTP13 hemizygous (81) and wild-type X1 females (80) ($P \leq 0.0001$), whereas AcTP13 homozygous females produced fewer eggs (84) than hemizygous (114) and WT-Mopti females (106) ($P \leq 0.003$). There were no statistically significant differences in fertility among the WT X1, WT-Mopti, and corresponding derived female lines. The variation in these data supports the conclusion that the differences found among the strains are not intrinsic to the drive system, but likely reflect unidentified or stochastic properties of WT-X1 and Mopti.

AgTP13 and AcTP13 Effector-Gene Impact on Reducing *P. falciparum*. m1C3 and m2A10 transcription controlled by the blood meal-inducible *AgCpA* and *AsVg1* gene promoters, respectively, is designed to drive their spatiotemporal expression to maximize their impact on different parasite stages. Previous studies showed that additional blood meals keep transcription elevated during the successive stages of parasite development and therefore three additional uninfected blood meals were supplied at 5, 9, and 11 d following the initial infectious meal to maintain m1C3 and m2A10 scFv levels (15, 16). This experimental design is supported by studies showing that some anopheline species, including *A. gambiae*, take several blood meals during each gonotrophic cycle, and ~70% of *A. gambiae* females in the laboratory take an additional blood meal within 24 h of the first meal, even when fully engorged, and 100% had an additional meal by the 6th day (41–44). Furthermore, the likelihood of a *Plasmodium*-infected mosquito taking multiple blood meals may be higher than that of an uninfected mosquito (43), further supporting the experimental design.

Hemi- and homozygous AgTP13 and AcTP3 adult females were offered blood meals supplemented with either low- and medium-concentration gametocyte cultures (gametocytemias of 0.01 to 0.03% and 0.03 to 0.08%, respectively). The lower gametocyte regimen produces oocyst mean intensities of infection (MII) consistent with what is observed in a number of naturally occurring infection levels in field-derived specimens and the medium regimen (or higher) is used often in laboratory experiments to enhance statistical power (16, 17, 21–22, 45–50). Summaries of all results and statistical analyses are provided in *SI Appendix*, Tables S23–S26.

Four biological replicates (experiments 1 to 4) were performed with AgTP13 and control lines (gene-drive only, AgNosCd-1; *cd*$^-$ mutant only, *Agcd*$^{\Delta 11,14}$) with the low gametocytemia (0.01 to 0.03%) regimen and the data presented pooled (Fig. 3 *A–D* and *SI Appendix*, Tables S23 and S24*A*) or individually (*SI Appendix*, Table S25). Both AgTP13 hemi- and homozygous adult females exhibited strong parasite suppression with oocyst prevalence reduced from ~74% in controls to 44.2% (hemizygotes, ~40% reduction) and 33.9% (homozygotes, ~54% reduction) (Fig. 3 *A* and *B* and *SI Appendix*, Tables S23, S24*A* and S25; $P < 0.0001$). Furthermore, oocyst MII decreased from 4.4 to 5.7 in controls to 2.0 and 1.2 in hemi- and homozygous females, with medians of zero (0) for both (control medians = 2.0 oocysts/midgut, $P < 0.0001$).

Importantly, AgTP13 females had significant reductions in the prevalence and MII of salivary gland sporozoites. Prevalence was reduced from 73 to 75% in controls to 42% (hemizygotes, ~43% reduction) and 31% (homozygotes, ~58% reduction), 2.4- and 1.8- fold respective decreases (Fig. 3 *C* and *D* and *SI Appendix*, Tables S23, S24*A* and S25; $P < 0.0001$). Furthermore, control MIIs were reduced from 4,007.5 per salivary gland pair to 1,832.5 and 759.6 in the AgTP13 females with control medians of 1,950 and 1,800 reduced to zero ($P < 0.0001$). Homozygous females show higher reductions of both midgut and salivary gland *Plasmodium* stages when compared to hemizygotes. All experimental samples had some mosquitoes with high sporozoite MIIs (up to 20,500 and 21,900 in hemi- and homozygotes, respectively), but only 2.9% (9/308) were ≥10,000.

Six biological replicates with hemi- and homozygous AcTP13 and control (AcNosCd-1 and WT-Mopti) females challenged with low and medium gametocytemia regimens were performed and scored separately. Pooled data from the two low gametocytemia replicates showed significant reductions in oocyst and sporozoite prevalence (Fig. 3 *E–H* and *SI Appendix*, Tables S23, S24*B*, and S26). Control oocyst prevalence of 72 to 78.3% was reduced to only 40% (~46% reduction) and 20.3% (~73% reduction) in the hemi- and homozygous females, respectively, with medians of 2 in controls and zero (0) in both hemi- and homozygous experimental females (Fig. 3 *E* and *F* and *SI Appendix*, Tables S23, S24*B*, and S26; prevalence and median intensities of infections $P < 0.0001$). Control oocyst MIIs were reduced from averages of 2.0 to 2.6 to 0.6 and 0.3 in the hemi- and homozygous females, respectively. Control sporozoite prevalence was reduced from ~77% to 26.2% (~66% reduction) and 18.5% (~76% reduction) in the hemi- and homozygous females, respectively (Fig. 3 *G* and *H* and *SI Appendix*, Tables S23, S24*B*, and S26; $P < 0.0001$). Females also show significant reductions in the MIIs from control levels of 2,635.6 sporozoites per salivary gland pair to 303.2 and 182.9 in hemi- and homozygous females, respectively ($P < 0.0001$). Median sporozoite numbers decreased from ~2,200 in controls to zero in both hemi- and homozygous females (*SI Appendix*, Tables S24*B* and S26; $P < 0.0001$). Similar to AgTP13, homozygous AcTP13 females have a greater impact on reducing *P. falciparum* infections with a 4.1-fold reduction of prevalence from an average of 77% in controls to 18.5% (~76% reduction). Although there were hemi- and homozygous AcTP13 mosquitoes with high numbers of parasites (ranging from 4,320 to 2,100, respectively), none (0/130) were ≥10,000.

AcTP13 females challenged with a medium gametocytemia level, 0.03 to 0.08%, had a lesser impact on reducing subsequent prevalence and MIIs (Fig. 3 *I–L* and *SI Appendix*, Tables S23, S24*C*, and S26). Oocyst prevalence was reduced moderately, but significantly, from ~97% in controls to 86.4% (~11% reduction) and 81.8% (~16% reduction) in hemi- and homozygous AcTP13 females, respectively (Fig. 3 *I* and *J* and *SI Appendix*, Tables S23, S24*C*, and S26; $P < 0.01$ and $P < 0.001$ for hemi- and homozygotes, respectively). However, both AcTP13 hemi- and homozygous females had MIIs, 11.5 and 10.2, respectively, lower than the control lines, which ranged from 24.2 to 27.4. The control medians were 17, 18, and 20 oocysts per midgut (WT-Mopti and AcNosCd-1 hemi- and homozygotes, respectively), while the AcTP13 hemi- and homozygous females had medians of 9 and 6, respectively (*SI Appendix*, Tables S24*C* and S26; $P < 0.0001$).

Sporozoite prevalence in salivary glands decreased from ~94% in controls to 67.8% (~28% reduction) and 62.1% (~34% reduction) in AcTP13 hemi- and homozygous females, respectively (Fig. 3 *K* and *L* and *SI Appendix*, Tables S23, S24*C*, and S26; $P < 0.0001$). The control MIIs decreased from 17,421 sporozoites per salivary gland pair to 6,261 and 5,692 in hemi- and homozygous females, respectively. Consistent with this, the median was reduced by ~91% from 13,650 in controls to 1,200 in AcTP13 homozygotes (*SI Appendix*, Tables S24*C* and S26; $P < 0.0001$). As seen previously, there was variation in sporozoite numbers among the individual mosquitoes sampled. Notably, 18.3%

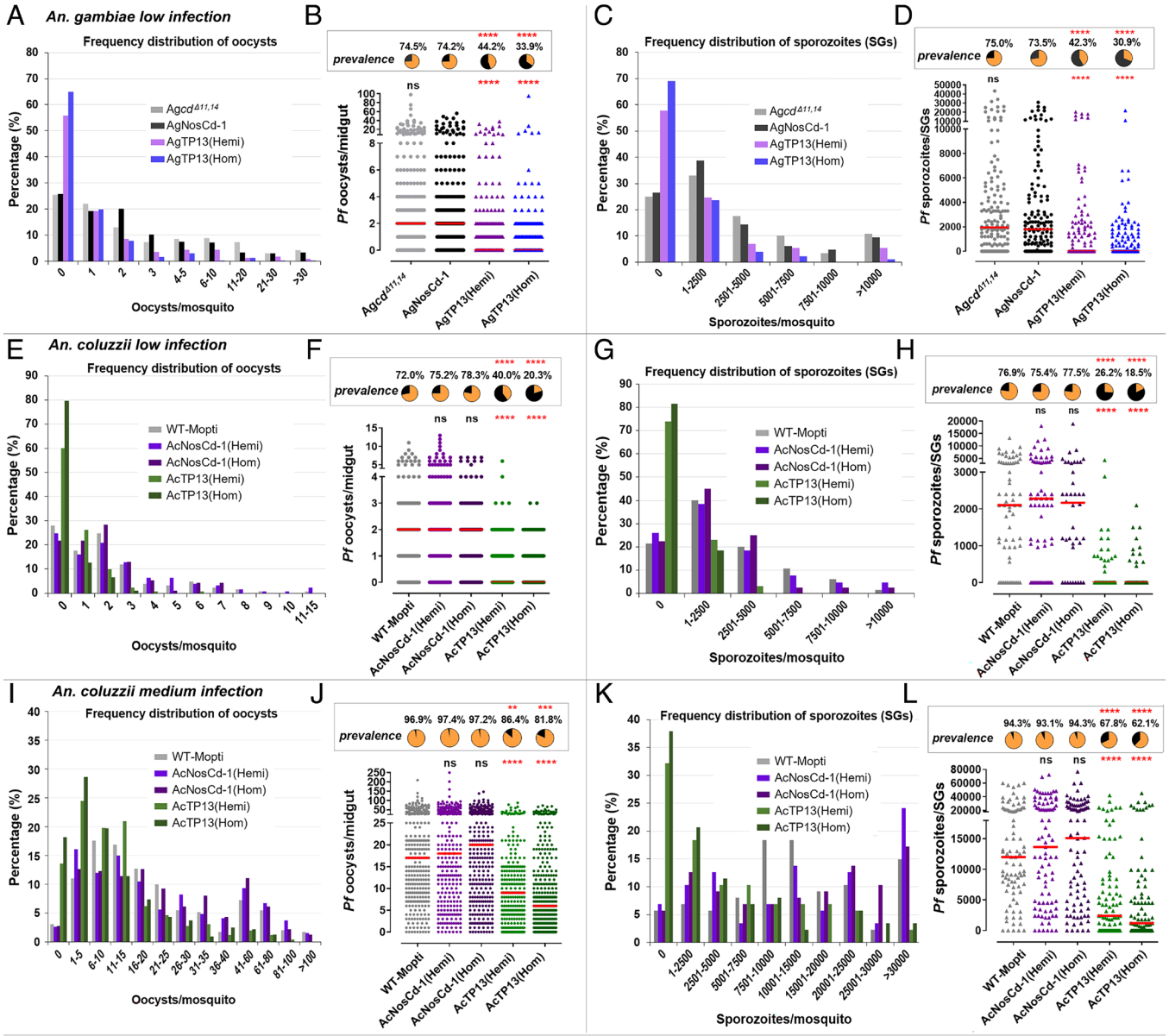

Fig. 3. *P. falciparum* (NF54) parasite prevalence and infection intensities in AgTP13 and AcTP13. Frequency distribution, prevalence and infection intensities of oocysts and sporozoites in hemi- and homozygous AgTP13 (*A-D*) and AcTP13 (*E-H*) challenged with low (0.01-0.03%) and AcTP13 (*I-L*) challenged with medium (0.03-0.08%) gametocytemia levels. Dot-plots and pie-charts display oocyst (*B*, *F* and *J*) and sporozoite (*D*, *H* and *L*) infection intensities and prevalence at 8 days post infection (dpi) in the midgut or 14 days dpi in the salivary glands, respectively. The *Agcd* mutant strain: *Agcd*$^{\Delta 11,14}$and AgNosCd-1 were used as controls for AgTP13, and WT-Mopti, AcNos*Cd*1(Hemi), and AcNos*Cd*1(Hom) were AcTP13 controls. The horizontal lines (red) indicate the median values. The Fisher's exact test was used to calculate *P*-values for infection prevalence and the Mann–Whitney test was used for median intensities of infections; **P* < 0.05; ***P* < 0.01, *** *P*< 0.001, *****P* < 0.0001.

(32/174) of the mosquitoes had ≥10,000 parasites (42,000 and 45,000 maxima in AcTP13 hemi- and homozygous females, respectively) in their salivary glands.

Modeling Potential Impact of TP13-Based Gene-Drive Strains on Malaria Parasite Transmission. The Mosquito Gene Drive Explorer 2 (MGDrivE 2) framework (24) was used to model conceptual field releases of TP13-based gene-drive strains. The model incorporates an "inheritance module" that describes the distribution of progeny genotypes for given maternal and paternal genotypes, a "life-history module" that describes the successive development of mosquitoes (eggs → larvae → pupae → adults) and an "epidemiology module" that describes pathogen transmission between mosquitoes and humans (*SI Appendix, Materials and Methods*).

AgTP13 and AcTP13 would never be released directly into the field. The TP13 gene-drive system would be introduced by mating or transgenesis into a recently colonized strain established from the planned field site. Therefore, a hypothetical strain, GCTP13, was patterned on the bionomics and seasonal population dynamics of local *A. gambiae* from the Grand Comore (GC) island, Union of the Comoros (*SI Appendix*, Table S27). The baseline malaria burden was modeled from the same location using data collected prior to the wide-scale implementation of control measures in 2006, with an initial (prerelease) ~36.4% prevalence and ~1.8 incidence (cases/1,000/day) (51, *SI Appendix*, Table S27). The life-table and male competitiveness analyses in *SI Appendix*, Table S21 are interpreted to indicate that there are no major loads affecting fitness that can be associated directly with the integration and expression of the gene-drive system.

Therefore, we maximized parsimony by modeling outcomes based on dominant gene-drive system fitness loads of 0, 10, and 20% for both GCTP13 hemi- and homozygotes. Values for the effector gene efficiencies were derived from the low and medium gametocytemia challenges of AgTP13 (GCTP13 *Ag*) and AcTP13 (GCTP13 *Ac*) (*SI Appendix*, Tables S23–S26).

The initial baseline target adult female mosquito population size, 75,000, is consistent with estimates from the Malaria Atlas Project (51) needed to produce the local mean malaria prevalence. Males are set to the same number for a total population size of 150,000. Other initial parameters are listed in *SI Appendix*, Tables S28 and S29. The release ratio of homozygous GCTP13 to WT males of 1:3.75 (20,000/75,000) was used in eight consecutive weekly releases for a cumulative total release ratio of 2.1:1. However, the ratio is expected to grow higher over the release period as the WT male numbers decrease due to mortality and the gene-drive male numbers increase from the emerging progeny of mated, drive-carrying females.

GCTP13 entomological modeling predicts that the experimentally observed, high gene-drive efficacy results in near-full modeling introduction (FMI) within 2 to 4 mo at all fitness loads following the final release with subsequent dynamics being determined by the load once the majority of WT alleles have been cleaved (Fig. 4 and *SI Appendix*, Figs. S6 and S7 and Table S30). FMI differs from the "full introduction" defined previously (every mosquito carrying at least one copy of the gene-drive system) and refers to the time it takes for ≥90% of the female mosquitoes to have at least one copy of the allele for ≥50% of the simulation repetitions. Based on the m1C3 and m2A10 antiparasite efficacy, this is consistent with a 65 to 90% reduction in vectorial capacity (35).

In the absence of a load (0), FMI is observed throughout the 6-y period. In contrast, the increase in the frequency of drive-resistant

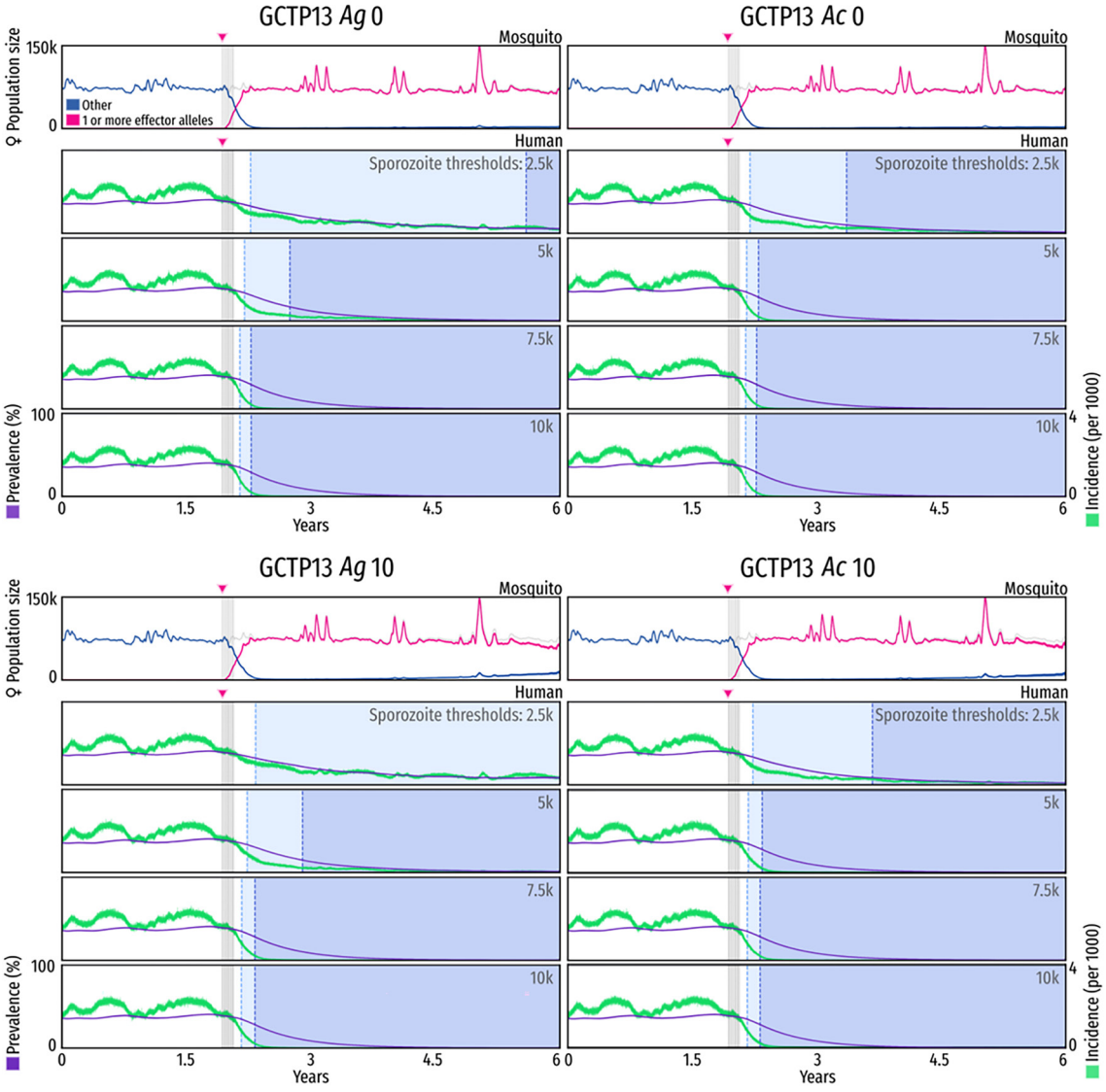

Fig. 4. Modeled entomological and epidemiological impacts following field releases of the hypothetical GCTP13 strains. Model parameters for mosquito bionomics, transmission-blocking efficacies, and malaria transmission use the inferred low gametocyte infection levels (*SI Appendix*, Tables S23–S26) and seasonal population dynamics resembling the island of GC, Union of the Comoros (*SI Appendix*, Tables S27–S29). (*Top*) mosquitoes carrying a 0% (0) fitness load. Mosquito: The size of the adult female mosquito populations in 1,000 s from 0 to 150 without (blue line) and with (red line) the drive systems along with the total (gray line) for GCTP13 *Ag* 0 and GCTP13 *Ac* 0 over multiple Years (1 to 6). The baseline adult female population size is ~75,000 for all simulations. The population size varies according to temperature effects on adult mortality and rainfall effects on larval carrying capacity. Eight consecutive weekly releases (light gray vertical bars) of 20,000 homozygous GCTP13 corresponding adult males begin 2 y (red arrows) into the simulation. Human: The modeled expected human malaria incidence (0 to 4 cases/1,000/day, green lines) and prevalence (0 to 100%, purple lines) before and after releases. Modeled outcomes are plotted for threshold levels (2.5 k, 5 k, 7.5 k, and 10 k) of *P. falciparum* sporozoites required for establishing a human infection. The light and dark blue-shaded regions represent time periods where human incidence is reduced by 50 to 90% and >90%, respectively. (*Bottom*) identical to *Top* panels with mosquitoes carrying a 10% (10) fitness load.

alleles at 40 to 42 and 24 to 26 mo following the final release of strains with 10 and 20% loads, respectively, begins to decrease the FMI due to the putative fitness advantage of functional resistant allele–carrying individuals over drive homozygotes (*SI Appendix*, Tables S18 and S30). Mosquitoes with the gene-drive system were absent at the end of the simulations (72 mo) with the 20% fitness loads.

The age- and mating-structured target wild population, competitive mating fitness, parasite challenge outcome data, and sporozoite threshold levels were used to predict the impact of the releases and presence of engineered mosquitoes on malaria incidence and prevalence. Consistent with the parasite challenge data, GCTP13 *Ac* strains outperformed GCTP13 *Ag* in all modeled scenarios. All strains with all fitness loads (0, 10, and 20%) calibrated with the low gametocytemia effector gene efficacies are predicted to have reduced incidence by 50 to 90% within 1 to 3 mo after the start of release at the 5, 7.5, and 10 k parasite infectivity threshold levels (Fig. 4 and *SI Appendix*, Fig. S6 and Table S30). The time to achieve the same incidence reduction was extended 2 to 4 mo after the final release for the 2.5 k parasite threshold simulations. Notably, GCTP13 *Ag* with the 20% fitness load went below the 50% incidence reduction level 39 mo after the final release. Reductions of >90% incidence were predicted within 3 to 6 mo after the start of release in all 0 and 10% fitness load simulations at the 7.5 and 10 k thresholds. Similar outcomes were predicted for GCTP13 *Ac* at the 5 k threshold, while it took 8 to 12 mo for GCTP13 *Ag* to achieve the same levels and the 20% fitness load for the latter resulted in the loss of this high level of reduction at ~34 mo. Fitness loads affected the 2.5 k simulation outcomes with the 0 load GCTP13 *Ag* achieving a >90% incidence reduction ~43 mo after the final release, while GCTP13 *Ac* achieved the same level in ~16 mo. GCTP13 *Ac* 10 and 20% fitness load strains took 20 to 23 mo to achieve the >90% incidence reductions for the 2.5 k threshold, whereas the corresponding GCTP13 *Ag* strains did not achieve these levels during the duration of the modeling. GCTP13 *Ac* with the 20% load dropped below 90% at ~30 mo.

Simulations were done with hypothetical GCTP13 *Ac* strains with the medium gametocytemia effector gene efficacies and the 0, 10, and 20% gene drive system fitness loads (*SI Appendix*, Fig. S6 and Table S30). All the 2.5 k threshold simulations failed to reach the 50% incidence reduction, and the 0 (5 k, 8.1 mo; 7.5 k, 3.3 mo; 10 k, 2.4 mo), 10 (5 k, 11.1 mo; 7.5 k, 4.4 mo; 10 k, 2.9 mo), and 20% loads (5 k, 24.9 mo; 7.5 k, 6.2 mo; 10 k, 3.8 mo) showed a delayed impact compared to the low gametocytemia simulations. This level of reduction was lost at ~27, 36, and 41 mo in the 20% load simulations for the 5, 7.5, and 10 k thresholds, respectively. Notably, the GCTP13 *Ac* 0 load simulation achieved a >90% incidence reduction at ~38 mo after the final release and remained there through the duration of the simulation.

Discussion

Generating the AgTP13 line was efficient and highly accurate, consistent with previous experience with Cas9/gRNA-mediated integrations of transgene cassettes (10, 11). The primary integration efficiency was comparable to that of the *piggyBac* transposable element with the advantage of inserting only a single copy of the transgene at a preselected site (52, 53). This supports the use of Cas9/gRNA-based technologies for the majority of mosquito transgenesis. Furthermore, once established in the WT-X1 strain, introgression into the Mopti strain was facilitated by the production of fertile hybrids following interspecific crosses, confirming other laboratory and field studies (54, 55).

The initial Cas9/gRNA-mediated conversion of drive-system mosquitoes from germline hemizygotes to homozygotes in *Anopheles* species is high, approaching and achieving 100% in males, with females being a few percent less (10, 11, 19, 40). Both AgTP13 and AcTP13 demonstrated high-efficiency gene drive in preliminary crosses and in the early generations of the cage trials, supporting the conclusion that the large cargo size did not reduce drive conversion efficiency, consistent with previous results in *A. stephensi* (40). While the starting conditions of each replicate of the cage trials were equivalent, stochasticity and male competitiveness affected the initiation and subsequent drive dynamics in individual cages. AcTP13 outperformed AgTP13 and showed rapid spread at both 1:1 and 1:3 male release ratios. AgTP13 did not spread as rapidly as AgNosCd-1, lagging by 2 to 3 generations in achieving full introduction in the 1:1 trials, but this difference was not as pronounced in the 1:3 release-ratio trials.

Critical to gene-drive performance is the ability of founding-generation males to contribute to the next generation. Assessments of life-table parameters showed that homo- and hemizygous AcTP13 males were as or more competitive than their wild-type rivals, whereas AgTP13 homozygotes were significantly less competitive. Interestingly, the competitiveness of hemizygous AgTP13 males was not statistically different from that of the wild types. Given the high rate of drive-mediated gene conversion, these males were mostly homozygous in their germ cells and hemizygous in their somatic tissues. The cage trials were initiated with somatically homozygous males and the observed competitive disadvantage of AgTP13 likely had an impact on delaying the time to full introduction. However, such a strain could be useful if it was reared to produce hemizygotes prior to its release. Importantly, TP13 is likely to perform better in other *A. gambiae* strains because the WT-X1 strain used here is derived from the *A. gambiae* G3 strain, which is known to exhibit a mixture of *A. gambiae* and *A. coluzzii* molecular markers (39), and there is anecdotal evidence based on our laboratory experience that this strain is not as robust as other long-colonized strains. Our follow-up work in *A. gambiae* will use recently colonized and molecularly verified strains of *A. gambiae sensu strictu*.

The evaluation of life-table parameters attempts to identify fitness loads that may affect the competitiveness of the gene-drive mosquitoes. The data also are useful in providing parameters for modeling the systems and their potential impacts. Similar to previous studies (11, 19), with the exception of the demonstrated competitiveness challenge of the homozygous AgTP13 males, no other life-table parameter alone stands out as being meaningful among AgTP13 and AcTP13 and their respective controls. Although statistically significant differences were found (some larval/pupal development times, larval viability, adult male longevity, and female fecundity), they varied among the lines and were not correlated with the presence of the gene-drive system. While these results appear unusual, inbreeding and selection in colonized laboratory strains are known to affect breeding (56, 57). In addition, some of the other life-table traits parameters may have benefited by a "line refreshment" that can occur when two long-standing independent laboratory lines are interbred (even if they share the same genetic background, such as G3 X1 and G3). The resulting offspring may exhibit improved overall fitness because negative loads in each line may be selected against and/or rescued by complementation. Homozygous AgTP13 males have shorter adult longevity compared to controls and the hemizygotes. It is possible that there is a load imposed by the knock-out of both copies of the target *Agcd* gene, producing nonfunctional alleles, and we are isolating functional and nonfunctional *cardinal* mutant strains to test this directly. However, drive system fitness impacts may be mitigated by the efficiency of gene conversion and may be overcome

by using higher release ratios (29, 58, 59). Mosquitoes from ongoing long-term cage trials will be evaluated after 1 y (~16 generations) to determine whether their life-table values are consistent with those determined here.

Previous work with anophelines showed that NHEJ-induced indels result principally from maternal effects as a consequence of the pre- and post-fertilization biology of developing eggs and embryos (10, 11, 19, 28). The resulting mutations may be resistant to further cleavage and therefore represent drive-resistant alleles. These alleles can affect drive dynamics and may cause a failure to achieve full introduction and result in mosquitoes that do not carry the system and effector molecules. Once most of the cleavable WT alleles in a population have been converted to gene-drive alleles, the drive system trajectory will determined by its fitness relative to individuals carrying functionally resistant target-site alleles. However, drive systems can cleave and convert wild-type alleles at high rates irrespective of fitness loads, and this competes with the processes that lead to the formation of resistance alleles. Heritable, drive-resistant alleles were found only in the AgTP13 cage trials and not in the AcTP13 replicates, although some were found in the progeny of CFP^{+}/cd^{-} AcTP13 mosquitoes from the female lineage of the founder and the maternal effect experiments. One 1:1 and all three 1:3 AgTP13 cage replicates had gene-drive dynamics affected by NHEJ drive-resistant alleles. Interestingly, all the three 1:3 cages had maximum introductions ≥90% before resistant alleles emerged in two of them. The lack of measured fitness costs for AcTP13 and perhaps even a fitness advantage are encouraging for long-term persistence, although such fitness measurements must be confirmed in the field.

Ongoing efforts are attempting to determine key features of *P. falciparum* transmission dynamics. The prevalence, intensities of infection, extrinsic incubation period (length of time needed for parasites to progress from gametocytes in the midgut to sporozoites in the salivary glands), number and duration of infectious bites per person, and reductions in human incidence are parameters represented in models and used here in our work (60–62). The observed impacts of the effector genes on prevalence and infection intensity are evaluated in the context of current discussions on thresholds. It is encouraging that both hemi- and homozygous AgTP13 and AcTP13 reduced prevalence in the single-generation low-gametocytemia challenges by amounts ≥32% of the threshold predicted as a prerequisite for malaria elimination (30). However, while some studies report MIIs of ≤5 oocytes per midgut (control averages in this study ranged from 2 to 5.7), these could be higher depending on seasonality, human infectious reservoir, and transmission intensity (number of infectious mosquitoes biting), and some report MIIs ≥10 (45–48). AcTP13 challenged with medium gametocytemias had oocyst MIIs of ~26. Not surprisingly, the reductions in prevalence were lower, 11 and 16%, for hemi- and homozygotes, respectively, not meeting the 32% threshold (30). None of the AcTP13 females in low-gametocytemia challenges were above the <10,000 sporozoite threshold (33–34) and only 2.9% of AgTP13 females were. However, 18.3% of the AcTP13 females in the medium gametocytemia protocol exceeded this threshold number and this was reflected in the modeling outcomes.

Nothing is known yet about the sporozoites seen in the low gametocytemia protocol. The dual effector strategy is designed to mitigate selection for parasite resistance, so these sporozoites most likely are in individual mosquitoes with low effector gene expression levels, presumably as a result of the impact of their blood meals on inducing expression. However, we are exploring methods to test these parasites to verify that they are not resistant to the scFvs. Furthermore, the results of laboratory-based membrane feeding assays using long-established parasite cultures are likely to differ from what occurs in the field. Current work with recently-derived diverse parasite cultures is in progress to determine whether laboratory results can be extrapolated reasonably to the field. It is also possible that long-term activity of the drive system in the target population could impair the effector molecules through mutation or aberrant recombination. We have long-term cage trials in progress to try and detect these possibilities.

The conceptual field release modeling provides support for further studies of TP13-based gene-drive systems, particularly regarding fitness impacts, parasite transmission-blocking efficacy, and drive-resistant allele formation. The modeling combines the laboratory-derived data collected here with features of a representative island field site to extrapolate potential epidemiological outcomes. The models make a number of assumptions (among them, that aside from fitness measurements, the laboratory performance of the lines reflects reasonably what might be expected in the field, and that parasite transmission is well described by a threshold model below which there is no transmission (30)), and highlight the significance of fitness loads and parasite transmission-blocking efficacy (as a function of sporozoite threshold and laboratory transmission intensity) on incidence and prevalence in humans. The more stringent threshold of a 50% incidence reduction was achieved in the simulations within 1 to 4 mo after the last release and was maintained for the duration at the low fitness loads (0 and 10%) and low gametocytemias for all sporozoite infections thresholds (2.5, 5, 7.5 and 10 k). The remarkable speed at which this threshold is reached is a function of the ability of the drive system to move rapidly into the target population. All simulations, except those for the 2.5 k sporozoite thresholds, also reach ≥90% reductions for at least 3 y. Simulations with the 20% fitness load and low gametocytemia all reached the 50% incidence reduction with the onset determined by the sporozoite infections thresholds. One simulation, GCTP13 Ag, provided an ~3-y ≥50% reduction level, but this did not last for the full duration of the simulation. The other five simulations all achieved the 90% incidence reduction for short or extended times. Not surprisingly, simulations with all three fitness loads (0, 10, and 20%) and medium gametocytemia showed longer times to achieve the 50% incidence thresholds for the 5, 7.5, and 10 k sporozoite infections thresholds (none achieved this for the 2.5 k threshold), but these were maintained for ≥3 y for the 0 and 10% fitness loads. The 20% fitness load resulted in a loss of this reduction by the end of the modeling period. Only the 0 fitness load achieved the ≥90% reduction during the last year of the simulation. Undoubtedly, if we had used the 20% reduction in incidence threshold, the modeled impacts would have been evident sooner and may have lasted longer in the more challenging simulations, but the 50% reduction appears to be an achievable target given the model assumptions. Previous and more recent modeling of similar and alternate population modification strategies also included parameters addressing seasonal impacts, as well as timing for release and the impact of the presence of preexisting vector control practices (insecticide-treated nets) in a grid-based conceptual sub-Saharan environments, and both identified circumstances that result in significant impacts on malaria epidemiology in a similar amount of time (63, 64).

The fitness parameters in the model aggregate potential loads that could result from insertion-site and transgene-expression effects. A parsimonious approach was chosen that assigned the same value (0, 10, or 20%) to both homo- and hemizygous drive-carrying mosquitoes and this is supported in part by recent work in crosses of drive-carrying and wild-type females to males homozygous for non-functional *cd* resistant alleles (28). However, future modeling is likely to include refinements that account for recessive insertion-site and

codominant expression effects that may be revealed in additional life-table analyses in different strains and these may affect the drive dynamics over multiple generations.

In summary, the coupling of gene-drive systems to antiparasite effector genes can produce laboratory-generated data for anopheline strains that can be used to inform complex epidemiological modeling of their potential impact on malaria incidence and prevalence. The TP13-based strains described here meet many of the minimally acceptable TPP thresholds and are eligible for further studies in anticipation of field trials.

Materials and Methods

Ethics Statement. All studies were performed in compliance with the requirements of the Guide for the Care and Use of Laboratory Animals of the NIH. The Institutional Animal Care and Use Committee at Johns Hopkins University approved the protocol (permit no. M006H300). Mice were used only as a blood source for mosquito rearing. Commercial anonymous human blood was used for *Plasmodium* gametocyte cultures and infection assays and informed consent was not required.

Details of all strains, reagents, and procedures are provided in *SI Appendix*.

Mosquito Strains and Lines. Wild-type lines: *Anopheles gambiae* G3 X1 (WT-X1) and *A. coluzzii* Mopti (WT-Mopti); transgenic lines: AgNosCd-1; *Agcd* mutant strain: $Agcd^{\Delta 11,14}$ (11, 28) are the sources of all insects used in this experiment.

Plasmid Design and Construction. The pCO37 plasmid (11) was used as a template to insert the m2A10 and m1C3 scFvs (15). The final plasmid, pTP13, contains all the pCO37 drive components linked to m2A10 and m1C3 (Fig. 1). The full sequences of the pTP13 components are listed in *SI Appendix*, Table S31.

Microinjection of Embryos and Screening Procedures. Microinjections were performed as described (9). Adult G_0 females and males were outcrossed to WT mosquitoes of the opposite sex and progeny screened for CFP fluorescence using UV-fluorescence microscopy.

Molecular Validation of Gene-Drive Cassette Integration and Effector Molecules Integrity. Genomic integration was verified by gene amplification analysis using genomic AgTP13 DNA as a template and gene-specific oligonucleotide primers (*SI Appendix*, Table S1).

Antiparasite Effector Expression Validation. Transcript accumulation and abundance were assayed using reverse-transcribed sex-, stage- and tissue-specific RNA samples and gene-specific oligonucleotide primers.

Initial Gene-Drive Mating. G_1 males and females were intercrossed in the presence of WT *A. gambiae* females to expand the colony. The six G_1 males were removed after 3 d and outcrossed to WT females. These two populations were subsequently maintained by intercrossing (IX; all CFP^+ progeny mated together) and outcrossing (OX; CFP^+ males mated to WT females) to generate homozygous and hemizygous lines.

Generation of the AcTP13 Line. AgTP13 (CFP^+/cd^-) males were outcrossed to female *A. coluzzii* WT Mopti. Progeny were recovered and F1 hybrids backcrossed to WT *A. coluzzii* Mopti females for five successive generations before mosquitoes were used in experiments.

Male and Female Lineage Gene-Drive Dynamics. Hemizygous AgTP13, AcNosCd-1, and AcTP13 males and females were outcrossed with WT mosquitoes of the opposite sex of the respective parental strain in a 1:1 ratio of 50 males to 50 females in three independent replicates. The progeny of these crosses were screened at the pupal stage for eye phenotypes and the presence or absence of the dominant fluorescent marker protein. Progeny from each lineage exhibiting a gene-drive hemizygous phenotype were removed, kept as virgins, and subsequently outcrossed to WT mosquitoes of the other sex. Male and female lineages were maintained for two generations to assess drive inheritance stability in each lineage.

Maternal Effect Analyses. Homozygous AgTP13, AcNosCd-1, and AcTP13 females were outcrossed to WT males of the respective parental strain in a 1:1 ratio in three independent replicates. Progeny were screened at the pupal stage and kept separate based on phenotype. Progeny with evidence of potential resistance alleles were intercrossed subsequently to assess drive dynamics and determine whether the evidence of resistance alleles in the eye would correlate to inhibition of drive in the individuals' germline.

Population Gene-Drive Dynamics. Cage trials were performed as described (11, 19, 40). AgTP13 and AcTP13 mosquitoes with exceptional phenotypes were collected individually and genomic DNA extracted. Gene amplification with target-specific oligonucleotide primers was used to verify the genotypes.

Life-Table Parameters. Life-table parameters were evaluated as described (11). Triple biological replicates were used for all experiments except the adult longevity for which ~100 mosquitoes per sex per line were monitored for survivorship.

***P. falciparum* Infection Assays and Statistical Analysis.** Hemi- and homozygous AgTP13 and control lines, AgNosCd-1 and $Agcd^{\Delta 11,14}$, and hemi- and homozygous AcTP13 and control lines, WT-Mopti, AcNosCd-1, were fed blood meals supplemented with NF54 strain *P. falciparum* gametocyte cultures as described (17, 21, 22). Dot plots of oocyst and sporozoite numbers in the midgut epithelium and salivary glands, respectively, were generated using GraphPad Prism 9 software, along with the MII and median values. *P*-values for infection intensities were calculated using the Mann–Whitney test, and Fisher's exact test was applied to the infection prevalence numbers (17, 21, 22).

Modeling. The MGDrivE 2 framework (24) was used to model the potential impact of the AgTP13 and AcTP13 lines on malaria transmission. A full description of the model and rationale for the parameter value assignments are included in *SI Appendix*.

Data, Materials, and Software Availability. All study data are included in the article and/or supporting information.

ACKNOWLEDGMENTS. We thank Drusilla Stillinger, Parrish Powell, Devin Nguyen, and Kiona Parker for mosquito husbandry; Rhodell Valdez for help in preparing the manuscript; and the Johns Hopkins Malaria Research Institute Insectary and Parasite Core Facility and the Bloomberg Philanthropies for the parasite challenge work. Funding was provided by the University of California Irvine Malaria Initiative and the Bill & Melinda Gates Foundation (INV-043645 to A.A.J.; INV-017683 to J.M.M.). A.A.J. is a Donald Bren Professor at the University of California, Irvine.

Author affiliations: [a]Department of Microbiology & Molecular Genetics, University of California, Irvine, CA 92697-4025; [b]W. Harry Feinstone Department of Molecular Microbiology and Immunology, Bloomberg School of Public Health, Malaria Research Institute, Johns Hopkins University, Baltimore, MD 21205; [c]Divisions of Epidemiology and Biostatistics, School of Public Health, University of California, Berkeley, CA 94720; and [d]Department of Molecular Biology & Biochemistry, University of California, Irvine, CA 92697-3900

1. S. Bhatt *et al.*, The effect of malaria control on Plasmodium falciparum in Africa between 2000 and 2015. *Nature* **526**, 207–211 (2015).
2. World Health Organization, "World malaria report 2022" (World Health Organization, Geneva, 2022), Licence: CC BY-NC-SA 3.0 IGO.
3. C. Sangbakembi-Ngounou *et al.*, Diurnal biting of malaria mosquitoes in the Central African Republic indicates residual transmission may be "out of control". *Proc. Natl. Acad. Sci. U.S.A.* **119**, e2104282119 (2022).
4. P. E. Duffy, J. P. Gorres, Malaria vaccines since 2000: Progress, priorities, products. *NPJ Vaccines* **5**, 48 (2020).
5. E. P. Caragata *et al.*, Prospects and pitfalls: Next-generation tools to control mosquito-transmitted disease. *Annu. Rev. Microbiol.* **74**, 455–475 (2020).
6. C. F. Curtis, P. M. Graves, Methods for replacement of malaria vector populations. *J. Trop. Med. Hyg.* **91**, 2 (1988).
7. R. Carballar-Lejarazú, A. A. James, Population modification of anopheline species to control malaria transmission. *Pathog. Glob. Health* **111**, 424–435 (2017).
8. F. Catteruccia *et al.*, Stable germline transformation of the malaria mosquito *Anopheles stephensi*. *Nature* **405**, 959–962 (2000).
9. R. Carballar-Lejarazú, T. Tushar, T. B. Pham, A. A. James, Microinjection method for *Anopheles gambiae* embryos. *J. Vis. Exp.* **173**, e62591 (2021).
10. V. M. Gantz *et al.*, Highly efficient Cas9-mediated gene drive for population modification of the malaria vector mosquito, *Anopheles stephensi*. *Proc. Natl. Acad. Sci. U.S.A.* **112**, E6736–E6743 (2015).

11. R. Carballar-Lejarazú *et al.*, Next-generation gene drive for population modification of the malaria vector mosquito, *Anopheles gambiae*. *Proc. Natl. Acad. Sci. U.S.A.* **117**, 22805–22814 (2020a).
12. D. A. Ellis *et al.*, Testing non-autonomous antimalarial gene drive effectors using self-eliminating drivers in the African mosquito vector *Anopheles gambiae*. *PLoS Genet* **18**, e1010244 (2022).
13. S. Yoshida *et al.*, A single-chain antibody fragment specific for the *Plasmodium berghei* ookinete protein Pbs21 confers transmission blockade in the mosquito midgut. *Mol. Biochem. Parasitol.* **104**, 195–204 (1999).
14. N. Xavier, A. A. James, Engineering Plasmodium-refractory phenotypes in mosquitoes. *Trend Parasitol.* **19**, 384–387 (2003).
15. A. T. Isaacs *et al.*, Engineered resistance to *Plasmodium falciparum* development in transgenic *Anopheles stephensi*. *PLoS Pathog.* **7**, e1002017 (2011).
16. A. T. Isaacs *et al.*, Transgenic *Anopheles stephensi* co-expressing single-chain antibodies resist *Plasmodium falciparum* development. *Proc. Natl. Acad. Sci. U.S.A.* **109**, E1922–E1930 (2012).
17. Y. Dong, M. L. Simões, G. Dimopoulos, Versatile transgenic multistage effector-gene combinations for *Plasmodium falciparum* suppression in *Anopheles*. *Sci Adv.* **6**, 20 (2020).
18. A. Hoermann *et al.*, Gene drive mosquitoes can aid malaria elimination by retarding Plasmodium sporogonic development. *Sci. Adv.* **8**, 38 (2022).
19. T. B. Pham *et al.*, Experimental population modification of the malaria vector mosquito, *Anopheles stephensi*. *PLoS Genet.* **15**, e1008440 (2019).
20. R. Carballar-Lejarazú, A. Kelsey, T. B. Pham, E. P. Bennett, A. A. James, Digital droplet PCR and IDAA for the detection of CRISPR indel edits in the malaria species *Anopheles stephensi*. *Biotechniques* **68**, 172–179 (2020b).
21. Y. Dong, F. Manfredini, G. Dimopoulos, Implication of the mosquito midgut microbiota in the defense against malaria parasites. *PLoS Pathog.* **5**, e1000423 (2009).
22. Y. Dong *et al.*, Engineered anopheles immunity to Plasmodium infection. *PLoS Pathog.* **7**, e1002458 (2011).
23. C. Sánchez *et al.*, MGDrivE: A modular simulation framework for the spread of gene drives through spatially explicit mosquito populations. *Methods Ecol. Evol.* **11**, 229–239 (2020).
24. S. L. Wu *et al.*, MGDrivE 2: A simulation framework for gene drive systems incorporating seasonality and epidemiological dynamics. *PLoS Comput. Biol.* **17**, e1009030 (2021), 10.1371/journal.pcbi.1009030.
25. A. A. James, S. James, J. Mumford, Y. Toure, "Progress and prospects for the use of genetically-modified mosquitoes to inhibit disease transmission. Report on planning meeting 1: Technical consultation on current status and planning for future development of genetically-modified mosquitoes for malaria and dengue control" WHO/TDR publications ISBN: 978 92 4 159923 8 (2010).
26. NASEM, National Academies of Sciences Engineering and Medicine, "Gene drives on the horizon: Advancing science, navigating uncertainty, and aligning research with public values" (Technical report, National Academies of Sciences Engineering and Medicine, The National Academies Press, Washington DC, USA, 2016).
27. S. L. James *et al.*, Pathway to deployment of gene drive mosquitoes as a potential biocontrol tool for elimination of malaria in Sub-Saharan Africa: Recommendations of a scientific working group. *Am. J. Trop. Med. Hygiene* **98** (suppl. 6), 1–49 (2018).
28. R. Carballar-Lejarazú, T. Tushar, T. B. Pham, A. A. James, Cas9-mediated maternal-effect and derived resistance alleles in a gene-drive strain of the African malaria vector mosquito, *Anopheles gambiae*. *Genetics* **221**, 2 (2022).
29. V. Bottino-Rojas, A. A. James, "Population modification using gene drive for reduction of malaria transmission" in *Transgenic Insects* 2nd Edition, M. Q. Benedict, M. Scott, Eds. (CABI Wallingford, UK, 2022), 243–258.
30. A. M. Blagborough *et al.*, Transmission-blocking interventions eliminate malaria from laboratory populations. *Nat. Commun.* **4**, 1812 (2013).
31. E. Ungureanu *et al.*, Prepatent periods of a tropical strain of Plasmodium vivax after inoculations of tenfold dilutions of sporozoites. *Trans. R. Soc. Trop. Med. Hyg.* **70**, 482–493 (1976).
32. N. Jasinskiene *et al.*, Genetic control of malaria parasite transmission: Threshold levels for infection in an avian model system. *Am. J. Trop. Med. Hyg.* **76**, 1072–1088 (2007).
33. M. Aleshnick, V. V. Ganusov, G. Nasir, G. Yenokyan, P. Sinnis, Experimental determination of the force of malaria infection reveals a non-linear relationship to mosquito sporozoite loads. *PLoS Pathog.* **16**, e1008181 (2020).
34. W. Graumans, E. Jacobs, T. Bousema, P. Sinnis, When is a Plasmodium-infected mosquito an infectious mosquito? *Trends Parasitol.* **36**, 705–716 (2020).
35. S. L. James, J. M. Marshall, G. K. Christophides, F. O. Okumu, T. Nolan, Toward the definition of efficacy and safety criteria for advancing gene drive-modified mosquitoes to field testing. *Vector Borne Zoonotic Dis.* **20**, 237–251 (2020).
36. A. Mondal, V. N. Vásquez, J. M. Marshall, Target product profiles for mosquito gene drives: Incorporating insights from mathematical models. *Front. Trop. Dis.* **3**, 828876 (2022).
37. G. Volohonsky *et al.*, Tools for Anopheles gambiae transgenesis. *G3 (Bethesda)* **5**, 1151–1163 (2015).
38. BEI Resources, BEI Resources Web Portal. https://www.beiresources.org/MR4Home.aspx. Accessed 21 June 2023.
39. Anopheles gambiae 1000 Genomes Consortium, Genome variation and population structure among 1142 mosquitoes of the African malaria vector species *Anopheles gambiae* and *Anopheles coluzzii*. *Genome Res.* **10**, 1533–1546 (2020).
40. A. Adolfi *et al.*, A population modification gene-drive rescue system dominantly eliminates resistance alleles in the malaria mosquito, *Anopheles stephensi*. *Nat. Commun.* **11**, 5553 (2020).
41. H. Briegel, E. Horler, Multiple blood meals as a reproductive strategy in *Anopheles* (Diptera: Culicidae). *J. Med. Entomol.* **30**, 975–985 (1994).
42. M. J. Klowden, H. Briegel, Mosquito gonotrophic cycle and multiple feeding potential: Contrasts between *Anopheles* and *Aedes* (Diptera: Culicidae). *J. Med. Entomol.* **31**, 618–622 (1994).
43. J. C. Koella, F. L. Sorensen, R. A. Anderson, The malaria parasite, *Plasmodium falciparum*, increases the frequency of multiple feeding of its mosquito vector, *Anopheles gambiae*. *Proc. Biol. Sci.* **265**, 763–768 (1998).
44. X. Nirmala, O. Marinotti, A. A. James, The accumulation of specific mRNAs following multiple blood meals in Anopheles gambiae. *Insect Mol. Biol.* **14**, 95–103 (2005).
45. R. Rosenberg, Malaria: Some considerations regarding parasite productivity. *Trends Parasitol.* **24**, 487–491 (2008).
46. B. P. Gonçalves *et al.*, Examining the human infectious reservoir for Plasmodium falciparum malaria in areas of differing transmission intensity. *Nat. Commun.* **8**, 1133 (2017).
47. J. Bradley *et al.*, Predicting the likelihood and intensity of mosquito infection from sex specific *Plasmodium falciparum* gametocyte density. *Elife.* **7**, e34463 (2018).
48. A. Bompard *et al.*, High Plasmodium infection intensity in naturally infected malaria vectors in Africa. *Int. J. Parasitol.* **50**, 985–996 (2020).
49. T. Bousema *et al.*, Mosquito feeding assays to determine the infectiousness of naturally infected Plasmodium falciparum gametocyte carriers. *PLoS One* **7**, e42821 (2012).
50. H. M. Soumare *et al.*, Maintaining Plasmodium falciparum gametocyte infectivity during blood collection and transport for mosquito feeding assays in the field. *Malar. J.* **20**, 191 (2021).
51. D. A. Pfeffer *et al.*, MalariaAtlas: An R interface to global malariometric data hosted by the Malaria Atlas Project. *Malar. J.* **17**, 352 (2018).
52. D. A. Amenya *et al.*, Comparative fitness assessment of Anopheles stephensi transgenic lines receptive to site-specific integration. *Insect Molec. Biol.* **19**, 263–269 (2010).
53. R. Carballar-Lejarazú, N. Jasinskiene, A. A. James, Exogenous gypsy insulator sequences modulate transgene expression in the malaria vector mosquito, *Anopheles stephensi*. *Proc. Natl. Acad. Sci. U.S.A.* **110**, 7176–7181 (2013).
54. M. C. Fontaine *et al.*, Mosquito genomics. Extensive introgression in a malaria vector species complex revealed by phylogenomics. *Science* **347**, 1258524 (2015).
55. B. Caputo *et al.*, Is Côte D'Ivoire a new high hybridization zone for the two major malaria vectors, Anopheles coluzzii and An. gambiae (Diptera, Culicidae)? *Infect. Genet. Evol.* **98**, 105215 (2022).
56. D. M. Menge *et al.*, Fitness consequences of *Anopheles gambiae* population hybridization. *Malar. J.* **4**, 44 (2005).
57. R. Baeshen *et al.*, Differential effects of inbreeding and selection on male reproductive phenotype associated with the colonization and laboratory maintenance of *Anopheles gambiae*. *Malar. J.* **13**, 19 (2014).
58. J. M. Ribeiro, M. G. Kidwell, Transposable elements as population drive mechanisms: Specification of critical parameter values. *J. Med. Entomol.* **31**, 10–16 (1994).
59. V. Macias, A. James, "Gene drive applications for mosquito control" in *Mosquito gene drives and the Malaria Eradication Agenda*, R. Carballar-Lejarazú, Ed. (Jenny Stanford Publishing, Singapore, 2022).
60. D. L. Smith *et al.*, Ross, Macdonald, and a theory for the dynamics and control of mosquito-transmitted pathogens. *PLoS Pathog.* **8**, e1002588 (2012), 10.1371/journal.ppat.1002588.
61. R. Ross, *The Prevention of Malaria* (Dutton, 1910).
62. G. Macdonald, "The epidemiology and control of malaria" in *The Epidemiology and Control of Malaria* (Oxford University Press, London, 1957).
63. P. A. Eckhoff, E. A. Wenger, H. C. Godfray, A. Burt, Impact of mosquito gene drive on malaria elimination in a computational model with explicit spatial and temporal dynamics. *Proc. Natl. Acad. Sci. U.S.A.* **114**, E255–E264 (2017).
64. S. Leung, N. Windbichler, E. A. Wenger, C. A. Bever, P. Selvaraj, Population replacement gene drive characteristics for malaria elimination in a range of seasonal transmission settings: A modelling study. *Malar. J.* **21**, 226 (2022).